Rare Metal Materials and Engineering
Volume 50, Issue 9, September 2021
Available online at www.rmme.ac.cn

Science Press

Cite this article as: Feng Rui, Wang Kelu, Lu Shiqiang, et al. Numerical Simulation of Unstable Deformation and Dynamic Recrystallization Behavior of BT25 Titanium Alloy During Hot Forging[J]. Rare Metal Materials and Engineering, 2021, 50(09): 3149-3157.

ARTICLE

Numerical Simulation of Unstable Deformation and Dynamic Recrystallization Behavior of BT25 Titanium Alloy During Hot Forging

Feng Rui, Wang Kelu, Lu Shiqiang, Li Xin, Zhou Xuan

School of Aeronautic Manufacturing Engineering, Nanchang Hangkong University, Nanchang 330063, China

Abstract: The thermal parameter boundary conditions of the unstable deformation microstructure and dynamic recrystallized microstructure of BT25 titanium alloy were determined by the instability maps and power dissipation maps, respectively. The results were used in the Deform-3D finite element (FE) software to effectively combine the processing map technique with FE technique. The FE codes after secondary development were used to simulate and predict the unstable deformation zones and dynamic recrystallization (DRX) behavior of BT25 titanium alloy at the deformation temperature of 950~1100 °C and the strain rate of 0.001~1 s^{-1}. The reliability of simulation results was verified by metallographic microstructure. Results show that the flow stress is decreased with increasing the deformation temperature or decreasing the strain rate. The unstable deformed microstructure is concentrated in the region of low temperature and high strain rate. Both high temperature and low strain rate are beneficial to DRX behavior. The results of metallographic microstructure are in good agreement with those of simulation, indicating that the method of combining processing map technique and FE technique is reliable and feasible for predicting the unstable deformed microstructure and DRX behavior in the metal forging process.

Key words: BT25 titanium alloy; instability map; power dissipation map; unstable deformation microstructure; dynamic recrystallization; numerical simulation

Because of the high specific strength and corrosion resistance at high temperature, titanium alloys have attracted extensive attention[1]. BT25 titanium alloy has good comprehensive performance, and its service life can reach 3000 h under high temperature environment of 550 °C. Currently, it is mainly used in the low-temperature region of aeroengines, such as the pressurized air cabin and casing and other important components of aero-engines[2-4]. With the rapid development of the aerospace industry, the demands of material properties are rising. The process determines the material microstructure which determines the material properties. Therefore, the forging process and microstructure control of BT25 titanium alloy have become the focus of research.

The unstable deformation and dynamic recrystallization (DRX) microstructures are the most common forged deformed microstructures in the process of hot machining, which play a decisive role in the mechanical properties of forgings[5,6]. The appearance of unstable deformed microstructure not only reduces the formability of metal, but also leads to uneven material properties. However, DRX behavior is conducive to grain refinement and homogenization. Therefore, the actual production conducts the overheat thermomechanical processing to control the microstructure. DRX method can not only avoid the unstable deformation structure, but also promote the grain refinement, thereby obtaining the excellent structure and material properties[7,8]. Therefore, it is very necessary to simulate and predict the unstable deformation and DRX behavior in the forging process, which is of great significance to improve the machinability of materials and to control the microstructure and properties of forgings.

With the rapid development of computer technology, finite element (FE) method and processing map technique are more

Received date: September 05, 2020
Foundation item: National Natural Science Foundation of China (51464035)
Corresponding author: Wang Kelu, Ph. D., Professor, School of Aeronautic Manufacturing Engineering, Nanchang Hangkong University, Nanchang 330063, P. R. China, E-mail: wangkelu@126.com

and more widely used. The FE method can simulate the microstructure evolution of metal materials in time and space dimensions. More and more scholars have combined the processing map technique with FE method. In the early stage, Sivaprasad et al[9] used FE software Marc2000 to simulate the thermal extrusion process of 304L stainless steel, combined the thermodynamic parameters with the micro-deformation mechanism in the machining diagram, analyzed the micro-deformation mechanism in the simulated thermal extrusion process, and optimized the process parameters. In recent years, Liu et al[10] proposed a new method for analysis of the machined magnesium alloy by thermal deformation, which combined FE method and three-dimensional machined maps, predicted the hot-forging experiment of magnesium alloy, and optimized the technical parameters. That method overcomes not only the problem that the thermal parameters of the unstable deformed and recrystallized deformed micro-structures predicted by the machining maps cannot be directly used to guide the actual forging production, but also the shortage that the FE technique cannot simulate or predict the deformed microstructure.

At present, the researches on BT25 titanium alloy are mainly focused on mechanical properties and process optimization. Ma et al[11] established the constitutive relation-ship of BT25 titanium alloy based on regression and artificial neural network (ANN) and predicted the flow stress by analyzing the results of the thermal compression tests of alloys. Yang et al[2] studied the high temperature plastic deformation behavior of BT25y alloy with initial equiaxed microstructure by thermal compression test. However, there are few reports on the numerical simulation of the instability processing maps and DRX behavior of BT25 titanium alloy. In this research, a novel method of combining the processing map technique with the FE technique was proposed for the simulation and prediction of the unstable deformed and DRX deformed microstructures during the forging of titanium alloy. The customized FE code implemented based on commercial software platform was used to simulate and predict the distribution and evolution of unstable deformation and DRX behavior of BT25 titanium alloy during thermal processing. Finally, the reliability of the model was verified by metallographic microstructure experiments.

1 Experiment

The experiment material is BT25 forged bar with a diameter of 200 mm and a height of 20 mm, and its main chemical composition is 7wt% AI, 2.2wt% Mo, 1.1wt% W, 1wt% Zr, and balanced Ti. The phase transus temperature of $(\alpha+\beta)/\beta$ is about 1026 °C, and the initial microstructure is duplex, as shown in Fig. 1. The volume fraction of α phase measured by quantitative metallography is 36.8vol%.

The specimens with dimension of Φ8 mm×12 mm were cut from the radial middle region of the forged bar by wire-electrode. The isothermal compression experiment of BT25 alloy was conducted by Gleeble-3500 thermomechanical simulator at the temperatures of 950, 980, 1010, 1040, 1070, and 1100 °C and the strain rates of 0.001, 0.01, 0.1 and 1 s^{-1}; and the maximum height reduction was 60%. The sub-transus temperature is 950~1010 °C and the super-transus temperature is 1040~1100 °C. Before the compression test, in order to reduce the friction between the specimens and die indenter, tantalum pieces should be added to both ends of the specimens. Specimens were resistance heated to the designed temperature at a heating rate of 10 °C/s. After the experiment, the specimens were quenched by water as soon as possible to retain the high temperature microstructures. Then the specimens were cut and inlaid along the axis, polished by sandpaper and polishing machine, corroded with a corrosion solution (HNO_3:HF:H_2O=1:2:5), and finally observed by optical microscope (OM).

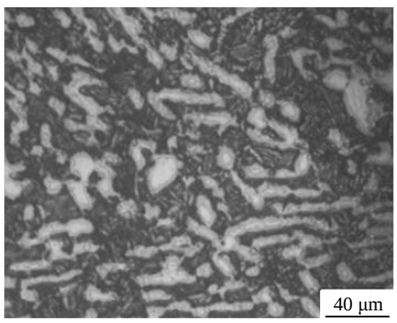

Fig.1 Original microstructure of BT25 titanium alloy

2 Flow Behavior of BT25 Titanium Alloy

Fig. 2 shows the true stress-true strain curves of BT25 titanium alloy at different deformation temperatures and strain rates. At the beginning of deformation, the flow stress is increased rapidly to the peak stress with increasing the true strain, and then it is decreased slowly and remains stable after reaching a certain true strain. This is mainly because in the early stage of thermal compression, work hardening takes the dominant position. With increasing the deformation temperature and true strain, the dislocation density is increased continuously, and the phenomenon of process softening effect begins to appear. Subsequently, the softening effect of processing takes the dominant position, and the flow stress decreases until the two effects are balanced and stable[12-15].

As shown in Fig. 2a and 2b, the flow stress is decreased with increasing the deformation temperature or decreasing the strain rate. On the one hand, the mobility at boundaries is higher and dislocation annihilation occurs more easily at the higher temperature, which promotes the phenomenon of dynamic softening effect. On the other hand, the lower strain rate provides more time for dynamic recovery and recrystallization, resulting in the lower work hardening[13,14].

3 Simulation and Prediction

3.1 Boundary conditions of instability deformation

According to the extremum principle of irreversible

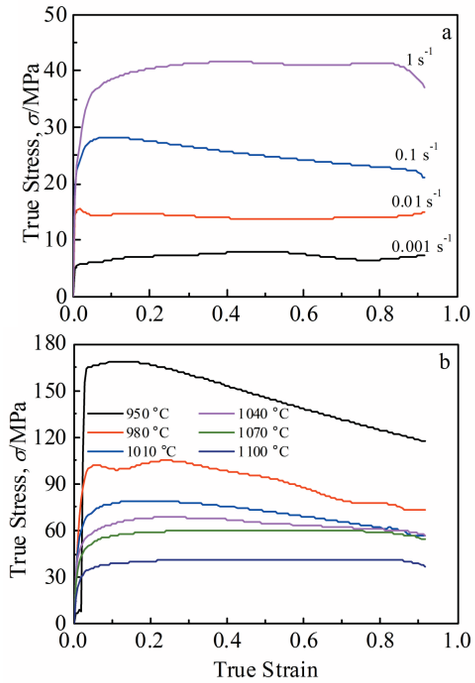

Fig.2 True stress-true strain curves of BT25 titanium alloy under different conditions: (a) deformation temperature=1100 °C; (b) strain rate=1 s^{-1}

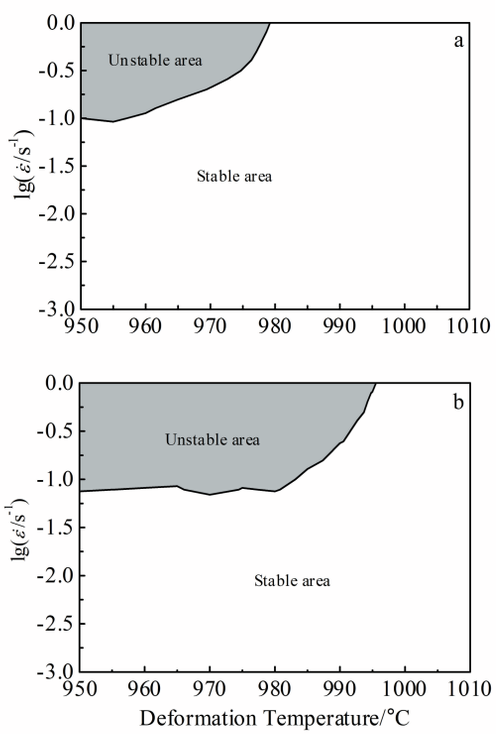

Fig.3 Instability maps at different strains: (a) ε=0.3 and (b) ε=0.9

thermodynamics of plastic rheology[16,17], if $\partial J/\partial\dot{\bar{\varepsilon}} > J/\dot{\bar{\varepsilon}}$, stable deformation appears. Conversely, instability deformation appears. The formula can be converted to Eq.(1) as follows:

$$\frac{\dot{\bar{\varepsilon}}\mathrm{d}J}{J\mathrm{d}\dot{\bar{\varepsilon}}} < 1 \rightarrow \frac{\mathrm{d}(\lg J)}{\mathrm{d}(\lg\dot{\bar{\varepsilon}})} < 1 \tag{1}$$

where $\dot{\bar{\varepsilon}}$ is equivalent strain rate; J is the dissipative covariance, representing the power consumption related to the microstructure change during the deformation process. J can be expressed by Eq.(2) as follows:

$$J = \int_0^{\bar{\sigma}} \dot{\bar{\varepsilon}}\mathrm{d}\bar{\sigma} = \frac{m\bar{\sigma}\dot{\varepsilon}}{1+m} \tag{2}$$

where m is the strain rate sensitivity index, $\bar{\sigma}$ is equivalent stress, and $\dot{\varepsilon}$ is strain rate. Take logarithm on both sides of Eq. (2), and then take the derivative with respect to $\ln\dot{\bar{\varepsilon}}$. The Prasad[18] criterion of instability deformation can be expressed as follows:

$$\xi(\dot{\bar{\varepsilon}}) = \frac{\partial\ln\left[m/(m+1)\right]}{\partial\ln\dot{\bar{\varepsilon}}} + m < 0 \tag{3}$$

The instability maps satisfy the variation of instability parameters $\xi(\dot{\bar{\varepsilon}})$ with strain rate and deformation temperature. According to the data of flow stress at different deformation temperatures and strain rates obtained from the isothermal strain rate compression experiment, the instability maps of BT25 titanium alloy under different strains were obtained based on the Prasad instability criterion. The areas of $\xi(\dot{\bar{\varepsilon}})$<0 are marked in gray, as shown in Fig. 3. The research scope of this section is in the two-phase area of α+β. Fig. 3 shows the instability maps at true strain of 0.3 and 0.9 and deformation temperature of 950~1010 °C. As shown in Fig. 3, the instability zones are mainly distributed in the low temperature and high strain rate zones. With increasing the strain, the instability deformation zones expand to the high temperature and low strain rate zones.

The instability superposition maps of the material were obtained by superposing the instability maps of all strains, as shown in Fig. 4. Because the deformed microstructure in the instability region is obtained from the instability deformed microstructure, the range of the instability region in the unstable superposition maps can be used as the boundary condition of the thermal parameters of the unstable deformation.

3.2 Simulation results of unstable deformed microstructure

The FE software of Deform-3D was programmed and the boundary conditions of thermodynamic parameters of the deformed microstructure obtained from the instability maps

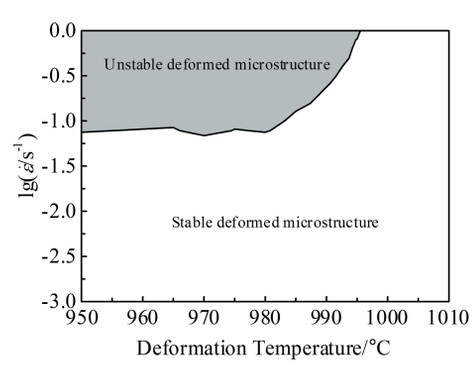

Fig.4 Superposition map of instability maps

were imported into the software. In the simulation, when the calculation result of a certain load deformation step converges, the thermal parameter field variables (temperature field, strain rate field, and strain field) in the deformation body are compared with the boundary conditions of the thermal parameters of the unstable deformed microstructure. If the thermal parameter field variables of a region in the deformation body is within the boundary condition of the thermal parameter of the unstable deformed microstructure, the region is determined as a unstable deformed microstructure, and its range is shown in the form of cloud graph. By analogy, the formation and evolution of unstable deformed microstructure in the process of thermal compression can also be simulated.

Fig.5 shows the simulation results of the unstable deformed microstructure in the constant strain rate compression process under different deformation parameters. In Fig. 5, the orange, yellow, and blue areas represent the stable deformed, unstable deformed, and undeformed microstructures, respectively. The simulated figures are ranged orderly according to the height reduction of specimens: 0%, 15%, 30%, 45%, and 60%. P1, P2, and P3 are the marking points of free deformation zone, difficult deformation zone, and large deformation zone in specimens, respectively. As shown in Fig. 5, when the deformation temperature is stable, the higher the strain rate, the larger the unstable microstructure area. In the early stage of thermal compression with the height reduction of 15%, a small amount of unstable deformed microstructure appears in the difficult deformation zone. With the development of deformation, the stable deformed microstructure area gradually shrinks and the unstable deformed microstructure area gradually expands.

Fig. 6 shows the equivalent strain rate variation curves of the material in different deformation zones under different deformation conditions. With increasing the height reduction, the equivalent strain rate in difficult deformation zone (P2)

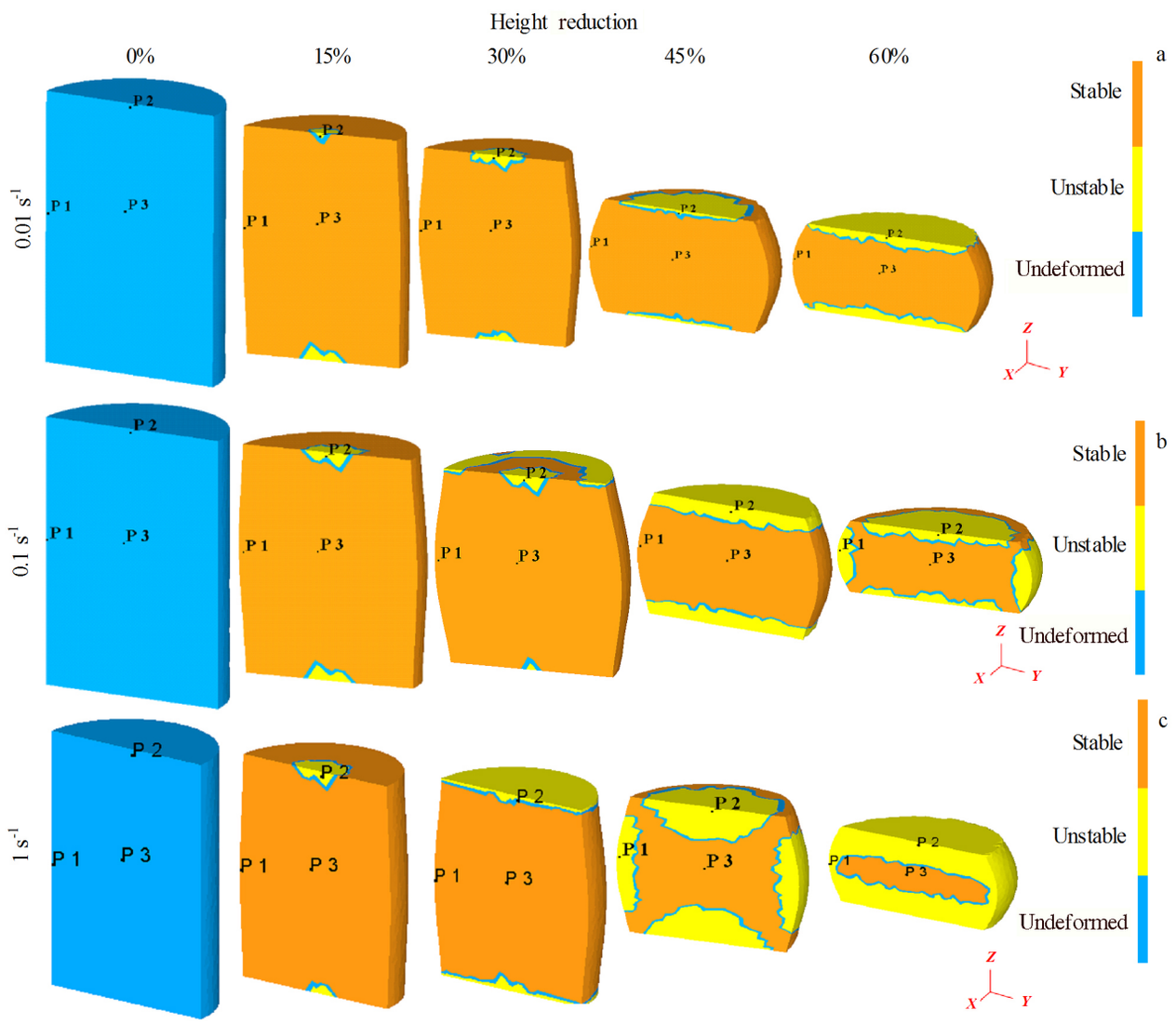

Fig.5 Simulation results of unstable deformed microstructure evolution during thermal compression of BT25 titanium alloy at 950 °C under different strain rates: (a) $\dot{\varepsilon}$=0.01 s^{-1}; (b) $\dot{\varepsilon}$=0.1 s^{-1}; (c) $\dot{\varepsilon}$=1 s^{-1}

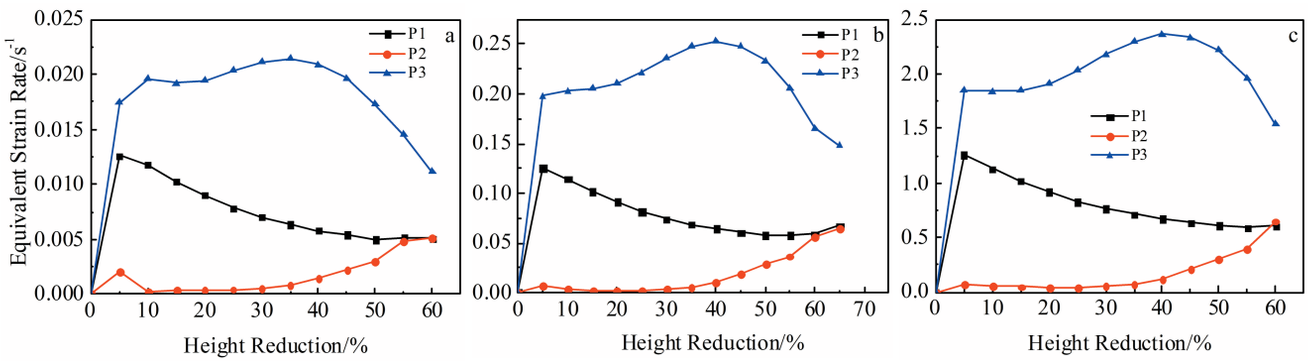

Fig.6 Equivalent strain rate variation curves of BT25 titanium alloy at 950 °C under different strain rates: (a) $\dot{\varepsilon}$=0.01 s^{-1}; (b) $\dot{\varepsilon}$=0.1 s^{-1}; (c) $\dot{\varepsilon}$=1 s^{-1}

rises slowly, while that in other areas increases firstly and then slowly decreases. Fig.6a indicates the decrement of strain rate in the large deformation zone is only 0.06 s^{-1} under the condition of strain rate of 0.01 s^{-1}, while that under the condition of strain rate of 0.1 and 1 s^{-1} is 0.09 and 0.07 s^{-1}, respectively. This result shows that the uniformity and coordination of the deformation are poor, which easily leads to the formation of unstable deformation microstructure.

3.3 Simulation results of DRX deformed microstructure

3.3.1 Power dissipation maps and thermodynamic parameters of DRX

According to dynamic material model (DMM) theory[19,20], the thermal deformation workpiece is a nonlinear power dissipation body, which can be regarded as an energy dissipation system during the material processing. The energy dissipation depends on the rheological behavior of material during processing. In the thermal processing, power P dissipation can be divided into two parts: visco-plastic heat G and microstructure evolution J, as expressed by Eq.(4):

$$P = \bar{\sigma}\dot{\bar{\varepsilon}} = G + J = \int_0^{\dot{\bar{\varepsilon}}} \bar{\sigma}\mathrm{d}\dot{\bar{\varepsilon}} + \int_0^{\bar{\sigma}} \dot{\bar{\varepsilon}}\mathrm{d}\bar{\sigma} \quad (4)$$

where G is energy dissipation, representing the power consumed by plastic deformation; $\bar{\sigma}$ is the equivalent stress. The power dissipation efficiency η[21] can be defined as follows:

$$\eta = \frac{J}{J_{\max}} = 2\left(1 - \frac{1}{\bar{\sigma}\dot{\bar{\varepsilon}}}\int_0^{\dot{\bar{\varepsilon}}} \bar{\sigma}\mathrm{d}\dot{\bar{\varepsilon}}\right) \quad (5)$$

where J_{max} is the maximum value of ideal linear energy dissipation (m=1) with $J_{max}=P/2$[22]; η is a dimensionless constant. For plastic deformation in the process of dynamic recovery, DRX and other microstructure deformations can cause the change of dissipation of J and η. The research scope of this section is in the single-phase area of β. The change of η at deformation temperature of 1040~1100 °C under different strains is shown in Fig. 7. The power dissipation maps under different strains can be obtained from Fig. 7. The characteristics of power dissipation maps under different strains are similar. The peak area of η does not change much in Fig. 7. The peak areas are concentrated at the low strain rate region. With increasing the strain rate, η is gradually decreased.

According to Ref.[2] and the microstructures, the peak area

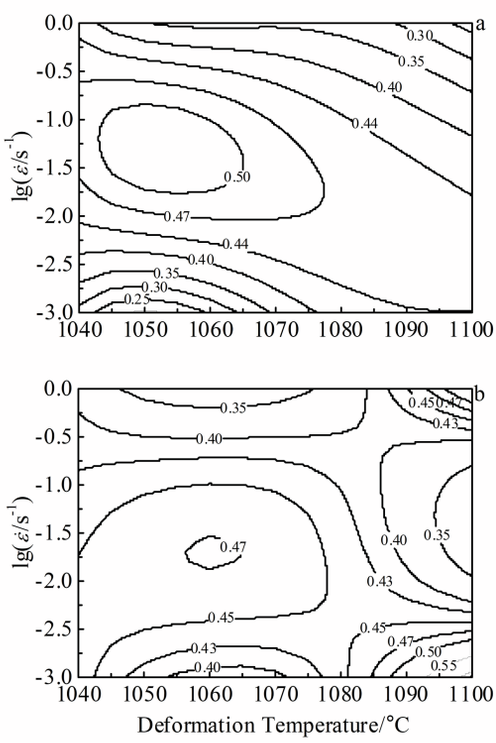

Fig.7 Power dissipation efficiency maps under different strains: (a) ε=0.3; (b) ε=0.9

of $\eta \geqslant 4.3$ is DRX deformed microstructure region, indicating that the micro-deformation mechanism of this region is DRX. Therefore, DRX thermodynamic parameter range of BT25 titanium alloy can be determined from the peak area in Fig. 8. The gray and white areas represent DRX structure and the non-DRX structure areas, respectively.

3.3.2 Critical strain of DRX

The critical strain of DRX refers to the true strain corresponding to the time when DRX occurs. It is important to determine the critical conditions for DRX to study the thermal processing of materials. In order to establish the critical strain model of BT25 titanium alloy, Najafizadeh[23] and Forouzan[24] models of work hardening rate were adopted in this research.

To determine the working hardening rate θ=dσ/dε of BT25 titanium alloy, the slope of each strain point on the true stress-

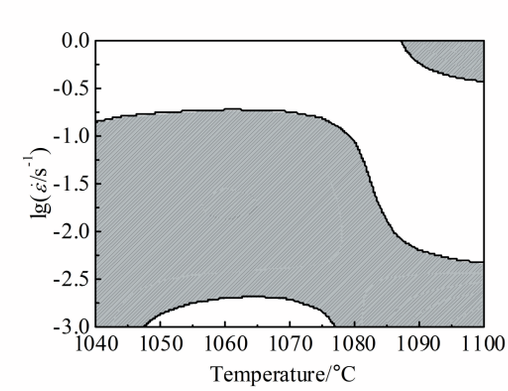

Fig.8 Thermomechanical parameters of DRX structure region of BT25 titanium alloy

strain curves needs to be calculated. Since the curves are not smooth, the fitting software was used with the strain difference $\Delta\varepsilon$=0.005 as the interval point. The deformation temperature of BT25 titanium alloy is 1070 °C, the strain rate is 0.01 s^{-1}, and the height reduction is 60%. Eq.(6) shows the 6-order fitting equation of the true stress-true strain curve with a fitting accuracy of 98.8%:

$$\sigma = \frac{0.367 + 437.67\varepsilon^2 - 4533.15\varepsilon^4 + 24\,511.38\varepsilon^6}{1 + 154\,978.96\varepsilon^2 - 194\,554.41\varepsilon^4 + 151026\varepsilon^6} \quad (6)$$

Eq. (6) is more complicated to calculate directly. Considering that the slope of two points is approximately equal to the slope of the fitting curve, the derivative can be taken and simplified as follows:

$$\ln\theta = -428.55\varepsilon^3 + 7316\varepsilon^2 - 39\,751.67\varepsilon + 9.57 \quad (7)$$

Using the negative derivative of Eq. (7), the relation between $-\partial\ln\theta/\partial\varepsilon$ and ε can be obtained, as shown in Fig.9a. It can be concluded that the strain corresponding to the lowest point of the curve is the critical strain (ε_c) which is 0.163 under this deformed condition. By analogy, the critical strain under all deformation conditions are calculated. The relation curves between critical strain and peak strain (ε_p) were calculated, and the fitting equation was obtained by the least square method, as shown in Fig.9b. It can be concluded from Fig.9b that the ratio of critical strain to peak strain is 0.63, which agrees with the data in Ref.[25].

The DRX critical strain model can be directly imported into the FE software as one of the thermodynamic parameter boundary conditions to judge DRX structure which only occurs at $\varepsilon>\varepsilon_c$.

3.4 DRX deformation simulation results

The program was developed again in Deform-3D software. The obtained power dissipation maps and DRX critical strain as boundary conditions of thermal parameters of DRX deformed microstructure were imported into the software. In the FE simulation, when the calculation result of a certain loading deformation step converges, the thermal parameter field variables (temperature field, strain rate field, and strain field) in the deformation body are compared with the thermal

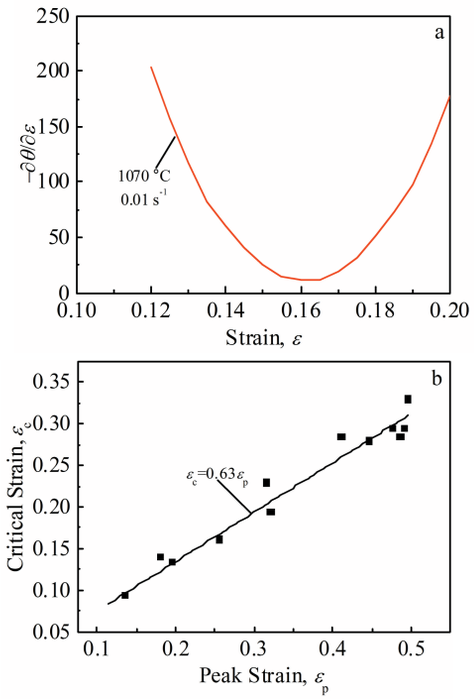

Fig.9 Relationship between $-\partial\ln\theta/\partial\varepsilon$-strain ε (a) and critical strain ε_c-peak strain ε_p (b)

parameter boundary conditions of DRX deformed microstructure. If the thermal parameter field variable of a region in the deformation body is within the boundary condition of the thermal parameter of DRX microstructure, and the true strain is greater than the critical strain ($\varepsilon > \varepsilon_c$), the region can be determined as DRX deformed zone and shown in the form of cloud graph. By analogy, the formation and evolution of DRX deformed microstructure in the whole forging process can be simulated and predicted.

Fig. 10 shows the simulation results of the unstable deformed zones in the compression process under constant strain rate and different deformation parameters. In Fig.10, the blue, red, and yellow regions represent the original microstructure, DRX microstructure, and non-DRX microstructure, respectively. The simulated figures are ranged orderly according to the height reduction of specimens: 0%, 15%, 30%, 45%, and 60%. P1, P2, and P3 are the marking points of free deformation zone, difficult deformation zone, and large deformation zone in specimens, respectively. As shown in Fig. 10, both low strain rate and high deformation temperature are conducive to the occurrence of DRX behavior. From Fig.10b and 10c, DRX occurs in both large deformation zone and free deformation zone with height reduction of 15%. As the strain increases, DRX region expands. In Fig. 10a, the specimen at low temperature and high strain only has non-DRX deformed microstructure during the whole compression process, indicating that no DRX occurs during the compression deformation under this deformation condition.

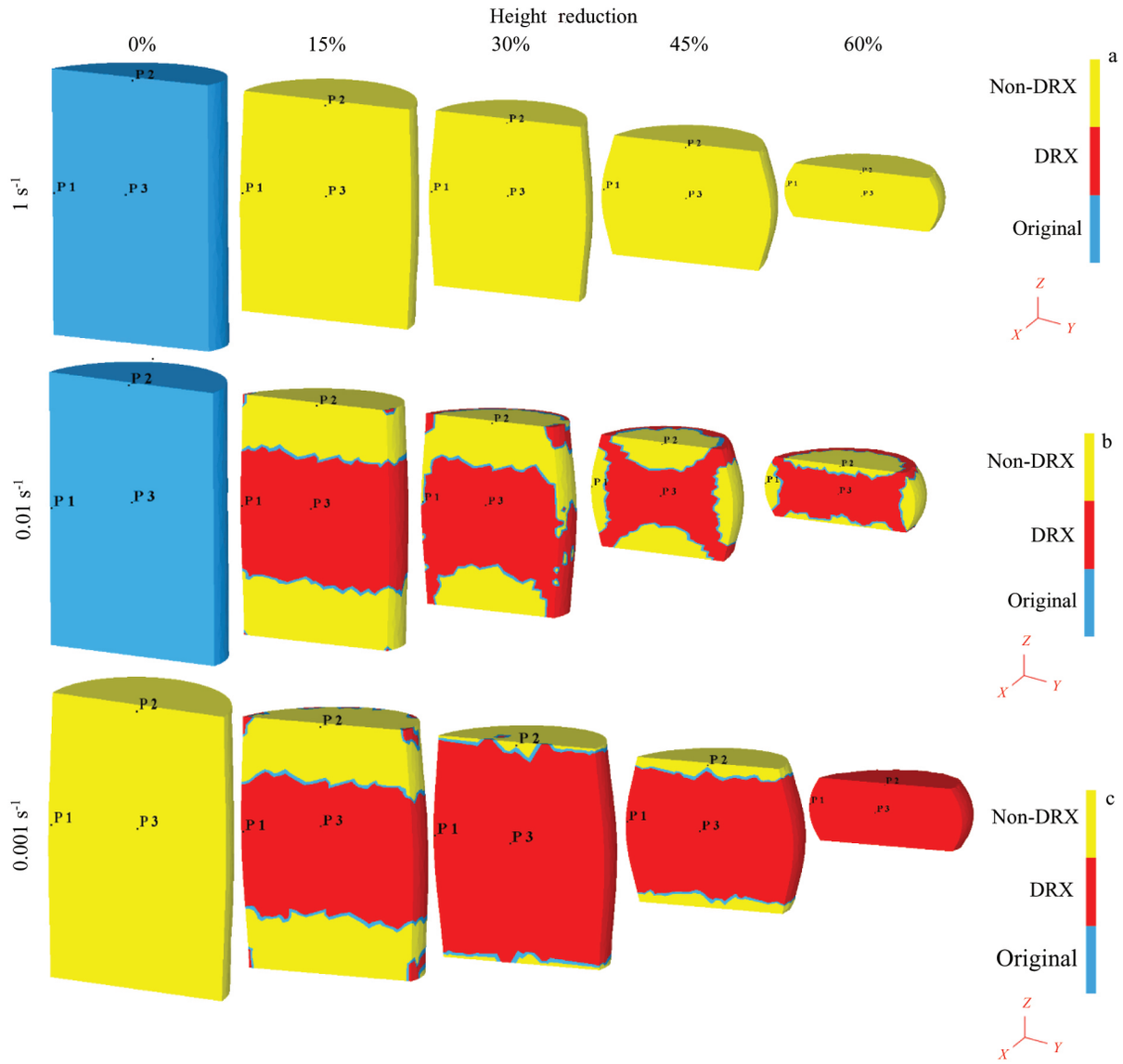

Fig.10 Simulation results of DRX microstructure evolution during thermal compression of BT25 titanium alloy under different deformation conditions: (a) T=1040 °C, $\dot{\varepsilon}$=1 s^{-1}; (b) T=1070 °C, $\dot{\varepsilon}$=0.01 s^{-1}; (c) T=1100 °C, $\dot{\varepsilon}$=0.001 s^{-1}

4 Experiment Verification

4.1 Verification of unstable deformed microstructure

In order to verify the accuracy of the simulation and prediction results about the unstable deformed microstructure, the specimen compressed with the deformation temperature of 950 °C, strain of 0.92, and strain rate of 1 s^{-1} was selected for further investigation. The metallographic observation was conducted on different deformation zones, and the results are shown in Fig.11. Fig.11b~11d represent the P1~P3 regions of the specimen, respectively. As shown in Fig. 11d, α and β phases in the microstructure of large deformation area are uniformly distributed. β phase is distributed around the α phase in a discontinuous state, and its boundary is irregular. Therefore, β phase is a stable deformed microstructure, as shown in Fig.11d. The local plastic flow phenomenon can be clearly observed from Fig. 11b and 11c. The α phase is distributed in a long strip along the flow direction, and the α and β phases are evenly distributed, indicating that the deformation under this condition results in unstable deformed microstructure.

In conclusion, when the deformation temperature is constant, the higher the strain rate, the larger the instability area. The conclusion is consistent with the simulation results, which verifies the reliability of the simulation method.

4.2 Verification of DRX deformed microstructure

In order to verify the accuracy of DRX deformation simulation and prediction results, the specimens compressed with the deformation temperature of 1070 °C, strain of 0.92, and strain rate of 0.01 s^{-1} was selected for further investigation. The microstructures of the compressed specimen in different zones were observed, as shown in Fig.12. As shown in Fig.12b and 12c, the grain boundary bending occurs, the grain is elongated, and the hard deformation zone shows

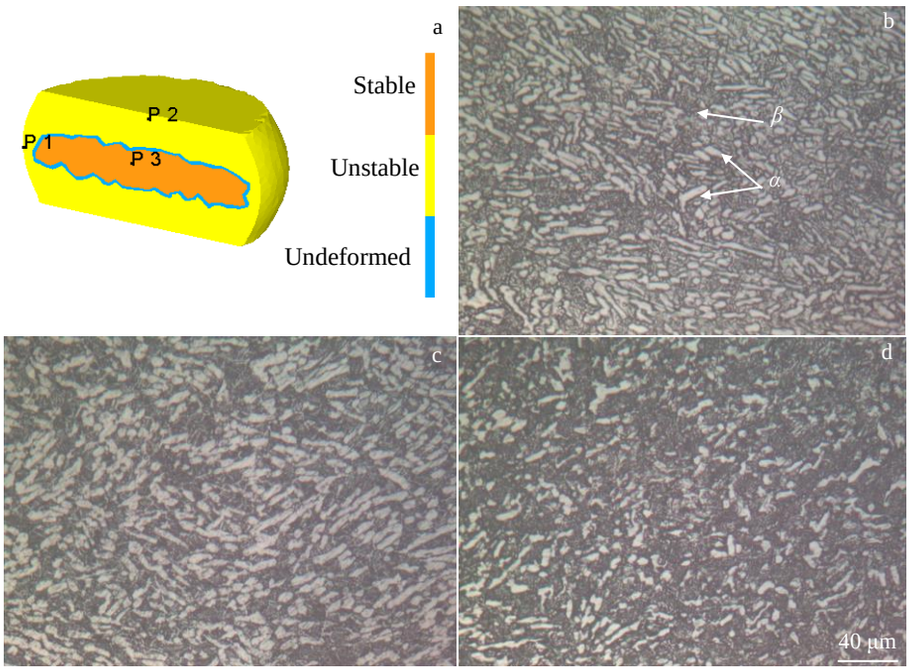

Fig.11 Simulation result (a) and OM images of P1 (b), P2 (c), and P3 (d) in Fig.11a of specimen deformed at 950 °C with strain of 0.92 and strain rate of 1 s^{-1}

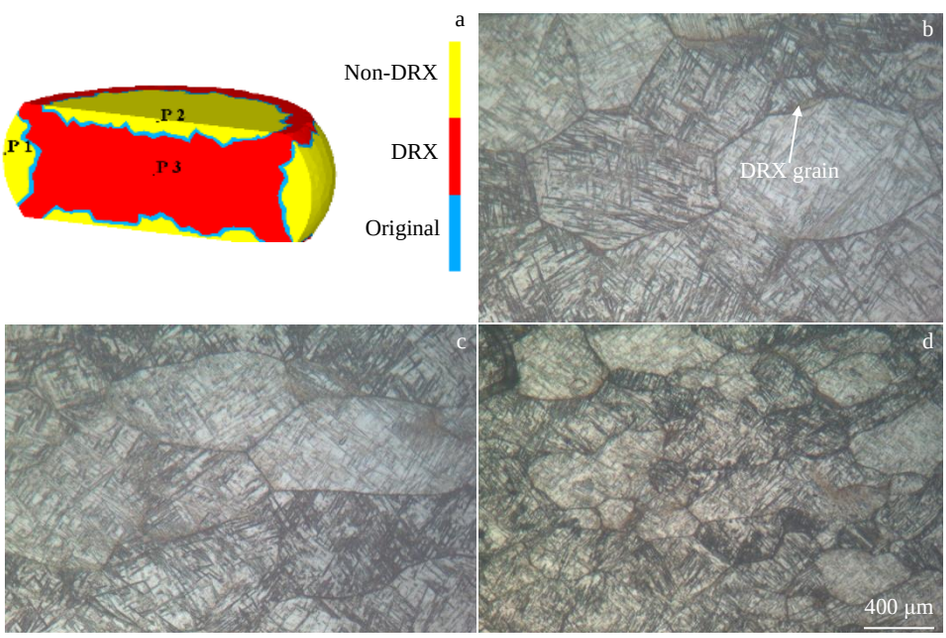

Fig.12 Simulation result (a) and OM images of P1 (b), P2 (c), and P3 (d) in Fig.12a of specimen deformed at 1070 °C with strain of 0.92 and strain rate of 0.01 s^{-1}

dynamic recovery characteristics. No DRX grains are observed, while nucleated and tiny DRX grains appear in the free deformation zone. The grain refinement in the large deformation zone is very obvious in Fig. 12d, and the recrystallization is sufficient, which agrees well with the simulation results.

Microstructure observations further suggest that this method combining the boundary conditions of the deformation determined by power dissipation maps and boundary conditions of DRX is feasible for predicting the DRX zones

during the metal forging.

5 Conclusions

1) The flow stress of BT25 titanium alloy is decreased with increasing the deformation temperature or decreasing the strain rate. The unstable deformed microstructures are concentrated in the areas of low temperature and high strain rate. Both high temperature and low strain rate are conducive to dynamic recrystallization (DRX) behavior.

2) The finite element (FE) software program was developed to simulate and predict the unstable deformed microstructure and DRX behavior of BT25 titanium alloy during the thermal compression process, which is verified to be feasible.

3) This method can also be used to simulate and predict the microstructure of other metals in the process of thermal processing, which provides guidance for industrial production and optimization of process parameters.

References

1 Dong Wang, Guo He, Ye Tian *et al*. *Journal of Materials Science & Technology*[J], 2020, 44: 160

2 Yang Xuemei, Guo Hongzhen, Yao Zekun *et al*. *Rare Metals*[J], 2018, 37(5): 778

3 Tian Yuxing, Liu Cheng. *Rare Metal Materials and Engineering* [J], 2019, 48(11): 3764

4 Wan Zhipeng, Sun Yu, Hu Lianxi *et al*. *Rare Metal Materials and Engineering*[J], 2018, 47(3): 835 (in Chinese)

5 Zhou Guowei, Li Zihan, Li Dayong *et al*. *International Journal of Plasticity*[J], 2017, 91: 48

6 Chen Xiong, Lv Yaping, Zhang Xiaoyong *et al*. *Rare Metal Materials and Engineering*[J], 2020, 49(3): 897

7 Taku S, Andrey B, Rustam K *et al*. *Progress in Materials Science* [J], 2014, 60: 130

8 Wang Zhongtang, Jiang Jihao, Liu Xunan *et al*. *Rare Metal Materials and Engineering*[J], 2019, 48(7): 2062

9 Sivaprasad P V, Venugopal S, Davies C H J *et al*. *Modelling and Simulation in Materials Science and Engineering*[J], 2004, 12(2): 285

10 Liu Juan, Li Juqiang, Cui Zhenshan *et al*. *Transactions of Nonferrous Metals Society of China*[J], 2013, 23(10): 3011

11 Ma Xiong, Zeng Weidong, Tian Fei *et al*. *Journal of Materials Engineering and Performance*[J], 2012, 21(8): 1591

12 Zhou Haiping, Zhang Hongbin, Liu Jie *et al*. *Rare Metal Materials and Engineering*[J], 2018, 47(11): 3329

13 Alireza H, Maryam M, Seyed M A *et al*. *Materials Science and Engineering A*[J], 2017, 681: 103

14 Wang Jingfeng, Xie Feizhou, Liu Shijie *et al*. *Rare Metal Materials and Engineering*[J], 2018, 47(6): 1700

15 Quan Sijia, Song Kexing, Zhang Yanmin *et al*. *Rare Metal Materials and Engineering*[J], 2019, 48(11): 3600 (in Chinese)

16 Venugopal S, Mannan S L, Prasad Y V R K. *Metallurgical and Materials Transactions A*[J], 1996, 27(1): 119

17 Luo Liangshun, Wang Fuxin, Wu Xiaoming *et al*. *Rare Metal Materials and Engineering*[J], 2018, 47(7): 2049 (in Chinese)

18 Gegel H L, Prasad Y V R K, Doraivelu S M *et al*. *AGARD Process Modeling Application to Metal Forming and Thermomechanical Process*[J], 1984, 11: 15 086

19 Venugopal S, Mannan S L, Prasad Y V R K. *Journal of Materials Science Letters*[J], 1997, 16(2): 137

20 Sun Huanying, Cao Jingxia, Wang Bao *et al*. *Rare Metal Materials and Engineering*[J], 2013, 42(11): 2351

21 Murty S V S N, Rao B N. *Journal of Materials Processing Technology*[J], 2000, 104(1-2): 103

22 Yang Qunying, Liu Wenyi, Zhang Zhiqing *et al*. *Rare Metal Materials and Engineering*[J], 2018, 47(2): 409

23 Najafizadeh A, Jonas J J. *ISIJ International*[J], 2006, 46: 1679

24 Forouzan F, Najafizadeh A, Kermanpur A *et al*. *Materials Science and Engineering A*[J], 2010, 527(27-28): 7334

25 Sellars C M, Whiteman J A. *Metal Science*[J], 1979, 13(3-4): 187

BT25钛合金在锻造过程中失稳变形和动态再结晶行为的数值模拟

冯　瑞，王克鲁，鲁世强，李　鑫，周　璇

(南昌航空大学 航空制造工程学院，江西 南昌 330063)

摘　要：分别利用失稳图和功率耗散图确定BT25钛合金失稳变形组织和动态再结晶变形组织的热力参数边界条件，并将其输入到Deform-3D有限元软件中，使加工图技术与有限元技术能够进行有效结合。利用二次开发后的软件对BT25钛合金在变形温度为950~1100 ℃和应变速率0.001~1 s^{-1}的条件下进行失稳变形组织和动态再结晶行为的模拟和预测，并通过对比金相组织，验证了该模拟结果的可靠性。结果表明，流动应力随变形温度的升高或应变速率的降低而降低；失稳变形组织集中在低温、高应变速率区域；高温和低应变速率均有利于动态再结晶（DRX）行为；微观组织的观察结果与模拟预测的结果吻合较好，说明本研究提出的加工图技术与有限元技术相结合的方法对模拟与预测金属锻造过程中的失稳变形组织和DRX行为是可行的。

关键词：BT25钛合金；失稳图；功率耗散图；失稳变形组织；动态再结晶；数值模拟

作者简介：冯 瑞，男，1993年生，硕士生，南昌航空大学航空制造工程学院，江西 南昌 330063，E-mail：13576076918@163.com